Mesh Generation for Turbomachinery Blade Passages with Three Dimensional Endwall Features

Feng Wang[a] and Luca di Mare[b]
Imperial College London, London, UK, SW7 2AZ

Turbomachinery blade passages are conventionally meshed by sweeping a mesh from a reference stream surface to other stream surfaces along the blade span. This approach is widely used in the gas turbine industry but it becomes problematic for simulations where the flow close to the endwall region is important. This is due to the fact that this approach has to make geometrical approximations for endwall features. This paper presents a method that overcomes this difficulty and generates optimal meshes for blade passages without geometrical approximations. The robustness of the method is demonstrated by meshing a multi-stage compressor with shroud cavities. Simulations of the compressor show the penalty of using meshes with approximated endwall features and the benefit of using meshes generated by the current method. These demonstrate that the proposed method contributes to the improvement of computational fluid dynamics as a reliable design tool for turbo-machines.

[a] Research Associate, Department of Mechanical Engineering.
[b] Lecture, Department of Mechanical Engineering.

Nomenclature

E = total internal energy [kg/J]

e = internal energy [kg/J]

g = covariant tensor [-]

H = total enthalpy [kg/J]

h = enthalpy [kg/J]

i,j = space indexing during navigation [-]

m,n = space indexing during navigation [-]

P = source function in the elliptic smoothing equation [-]

p = pressure [Pa]

R = gas constant [J/(kg $\cdot$ K)]

S = strain rate [1/s]

T = temperature [K]

t = time [s]

v = velocity [m/s]

x = spatial coordinate [m]

γ = Ratio of specific heats [-]

δ = Kronecker delta [-]

ε = spatial coordinate in the computational space [-]

κ = thermal conductivity coefficient [W/(m $\cdot$ K)]

μ = molecular viscosity [kg/(s $\cdot$ m)]

μ_t = turbulent viscosity [kg/(s $\cdot$ m)]

τ = shear stress [Pa]

τ^t = turbulent shear stress [Pa]

ρ = density [kg/m^3]

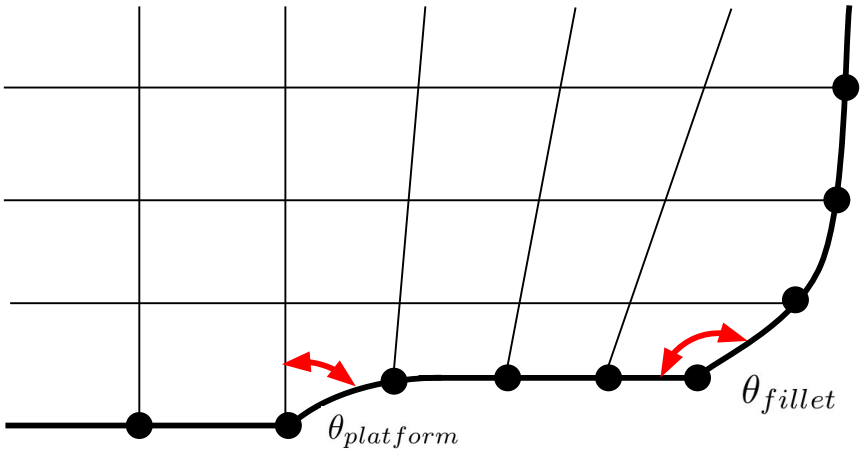

Fig. 1 Geometrical approximations by the 2.5D approach.

I. Introduction

Computational Fluid Dynamics (CFD) has found wide application in the gas turbine industry. It has become an essential design and analysis tool. CFD requires a mesh to decompose the model geometry into a tessellation of polytopes (e.g. quadrilateral in 2D and hexahedra in 3D). The quality of a mesh is one of the main elements that decides the success of CFD simulations. The focus of this paper is on the mesh generation of turbomachinery blade passages.

Multi-block structured meshes are traditionally preferred in simulating blade passages because of their accuracy and easy-to-use data structures where CFD algorithms can be greatly simplified (e.g. multigrid). Although the mathematical foundation for 3 Dimensional (3D) multi-block structured meshing is well established [1], the techniques of generating multi-block structured meshes for turbomachinery blade passages have not evolved significantly from stacking a set of surface meshes along the blade span [2–4] in the past decade. This is based on the observation that the geometries of blade passages can be treated as 2.5 Dimensions (2.5D). A 2.5D geometry means a geometry is 3D, but it can be generated by sweeping a surface from a source surface to a target surface. This reduces the problem of meshing a 3D blade passage into a set of 2D meshing problems on the stream surfaces. Furthermore this approach lends itself naturally to the computation of useful quantities such as mass averages.

The disadvantage of the 2.5D approach is its assumption that the geometries of blade passages are 2.5D. Figure 1 illustrates the truncated fillet and the platform edge with the 2.5D approach.

θ_{fillet} has to be sufficiently smaller than 180^o so that the element close to the fillet have acceptable quality. $\theta_{platform}$ is also required to be larger than 0^o to some extent. For many turbomachinery applications, these 3D geometrical features are essential to obtain accurate predictions of the flows near endwall regions. Previous studies have shown that blade fillets and shroud leakage flows have significant impact on the performance of turbomachines [5, 6]. Unfortunately due to the limitations of the 2.5D approach, these 3D features can only be approximated in order to obtain a valid mesh with acceptable quality.

In order to resolve these 3D geometrical features, prismatic hybrid meshes can be used for turbomachinery blade passages [7]. However, flows within turbomachinery blade passages exhibit an obvious direction and the mesh elements in the hybrid mesh are generally not aligned with the flow direction, so the solution obtained from a hybrid mesh tends to be diffusive using industrial CFD codes. Even though adaptive and anisotropic meshes can be generated to align the meshes with flow directions to reduce numerical errors, they are rarely used to mesh turbomachinery blade passages in the industry. Furthermore, on the exit and inlet boundaries special techniques are required to group elements at different radial positions for the mixing plane approach. Therefore hybrid meshes are only considered if generating multi-block structured meshes is no longer a feasible approach (e.g. meshing the nozzle guide vanes with cooling slots) [7].

A method [8] has recently been proposed to build fully 3D multi-block structured meshes for turbomachinery blades with fillets. The method is capable of meshing the blade fillet with no approximations but the treatment of other endwall features (e.g. the shape of the platform) is not covered. The capability of the method is demonstrated with blades lacking modern 3D design features, such as sweep and dihedral, therefore the robustness of the method to handle modern turbomachinery blades is dubious.

Gas turbine designers require that CFD simulations are able to provide accurate predictions of performance, stall margin and stage matching. This mainly relies on the capability of the CFD solver (e.g. turbulence and blade row interactions) and the accuracy of the geometry. The 2.5D approach will remain useful in meshing blades where the effects of blade fillets and platform leakage flows are marginal. However, because of the approximations made by this approach, the endwall

geometries cannot be modelled accurately. This undermines the effort of improving the CFD solvers to enhance the reliability of CFD in simulating blade passages where endwall regions are crucial. Therefore, there is a need to develop a meshing tool to resolve these geometrical features with no approximations and the meshing tool is preferred to generate multi-block structured meshes. The contribution of this paper is to address this need. The proposed method extends the 2.5D approach to a fully 3D approach and generates multi-block structured meshes with optimal quality to handle 3D endwall geometrical features.

II. Methogology

A. Constructing 3D Blocks

After the surface meshes are generated, 3D blocks are generated in the blade passage. This is demonstrated by the schematic in Fig. 2. The surface mesh of the blade which is highlighted in red in Fig. 2 is extruded in the normal direction to generate the block for the boundary layer mesh on the blade. The extrusion will result in a modified blade surface, which is highlighted in orange in Fig. 2. In the rest of the domain, the 2.5D approach is used by sweeping the surface mesh from the hub to the casing. For a stator blade, the surface meshes on both endwalls are swept in the normal direction for the boundary layer mesh. This step is marked as "sweep1" in Fig. 2 a). The resulting blocks will have a point-to-point matching on the interfaces with the blocks on the blade surface. In the rest of the domain, the blocks are generated by sweeping the surface mesh of the extruded blocks from endwalls. These surface meshes are highlighted in dashed blue lines. This step is marked as "sweep2" in Fig. 2 a). For a rotor blade, due to the existence of the tip gap clearance, only blocks on the hub are extruded from endwalls and this step is marked as "sweep1" in Fig. 2 b). In the rest of the domain, the blocks are generated by sweeping the surface meshes (highlighted in dashed blue lines) of the extruded blocks from the hub to the casing. The step is marked as "sweep2" in Fig. 2 b). It is worth mentioning that the background meshes on the inlet and exit boundaries generated by the 2.5D approach is required to guide the sweeping. This ensures that the mesh of the current blade row does not intersect with meshes of neighbouring blade rows.

For blades with shroud leakage slots, the construction of 3D blocks is illustrates in Fig. 2 c). On the interface of the hub and the shroud leakage slot, extrusion of the boundary layer meshes

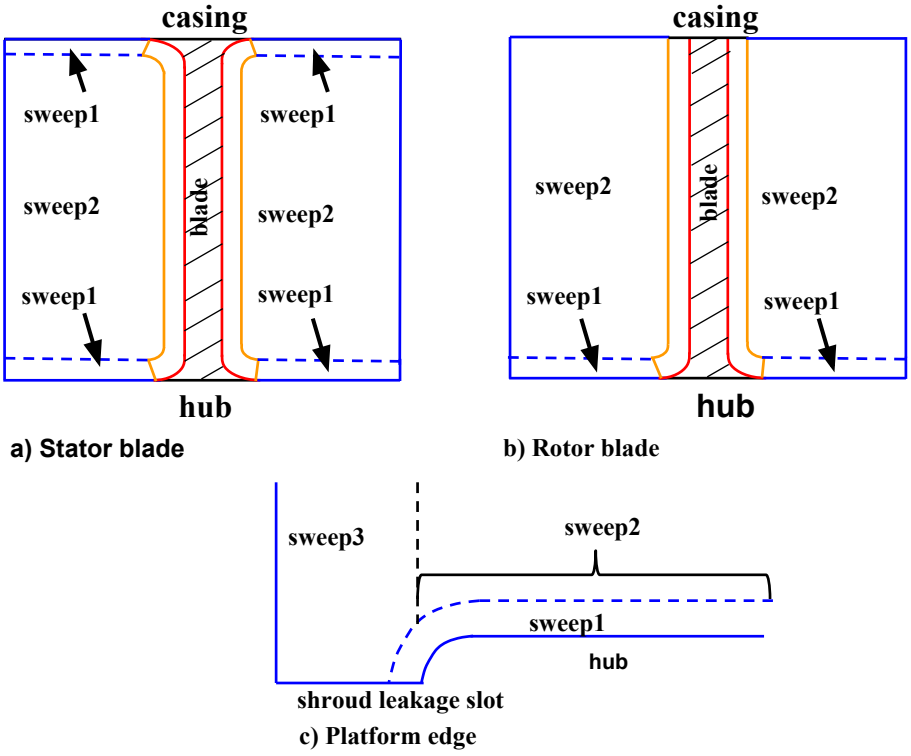

Fig. 2 Illustration of block constructions.

("sweep1" in Fig. 2 c)) follows the surface of the leakage slot. 3D blocks in the rest of the domain are generated by 2 steps. The first sweep ("sweep2") uses a fraction of the the extruded surface mesh from the hub, which is highlighted in Fig. 2 c). The second step ("sweep3") sweeps the mesh from the shroud leakage slot to the casing.

On the pitch-wise direction, the block layout will resemble the block layout of the 2.5D approach, therefore optimal block layouts for different blades in the 2.5D approach can be reused in the current method. Figure 3 demonstrates the blocks for a compressor passage with shroud leakage slots. Figure 3 a) shows an overview of the blocks. Figures 3 b)-c) present the projection of the 3D blocks on a stream surface and a close-up view of blocks around the platform.

After the blocks are generated, algebraic meshes are generated in each block using 3D Transfinite Linear Interpolation (TFI) [9]. Grid folding will be present in this initial mesh and they will be removed by elliptic smoothing.

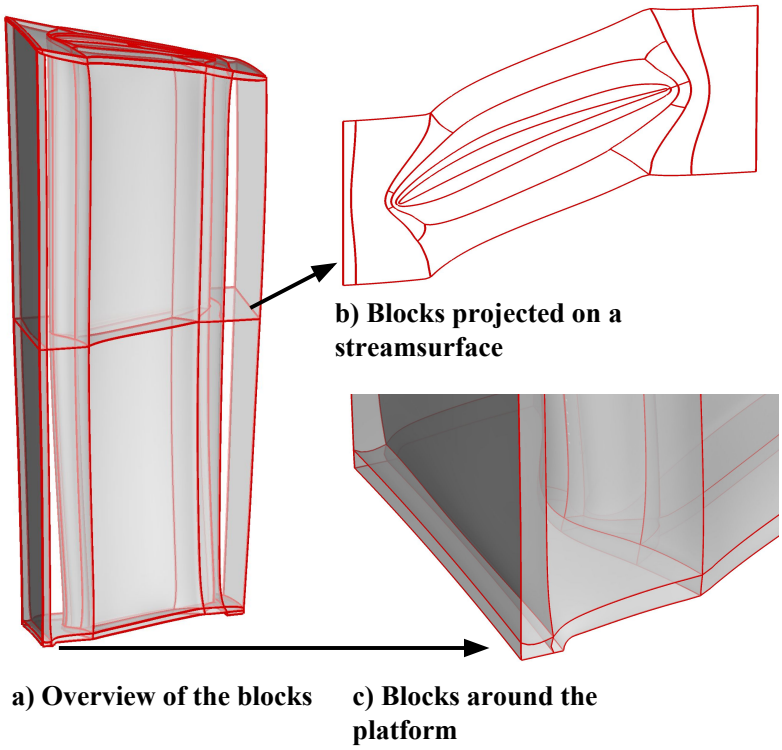

Fig. 3 3D Blocks for a stator passage

B. Stitching 3D Blocks

Before the elliptic smoothing is applied, the blocks are stitched together. The entities at the intersection between two or more blocks are termed as stitch surfaces, stitch lines and junction points. Their constructions are based on the following three properties: 1) One-to-one matching on the periodic boundary. 2) No hanging point in the blocks. For a block B_i and the surface mesh on the j^{th} block boundary ∂B_{ij}, $\forall p \in \partial B_{ij}$, a point $p^* \in \partial B_{kl,k\neq i \vee l \neq j}$ can always be found such that p and p^* have the same coordinates. 3) Mismatch among block interfaces are allowed if no hanging points are produced.

Based on these properties, once all the blocks are constructed the stitch surfaces, stitch lines and junction points can be built automatically by looping through all the blocks and their boundaries. Junction points are the points where stitch lines meet and stitch lines are the lines that join stitch surfaces together. A stitch surface is a subset of a block boundary that is shared by two blocks. Stitch surfaces are built by matching the block boundaries and they can be built by the following three ways: 1) One-to-one matching. This is the trivial situation when the boundaries of two blocks

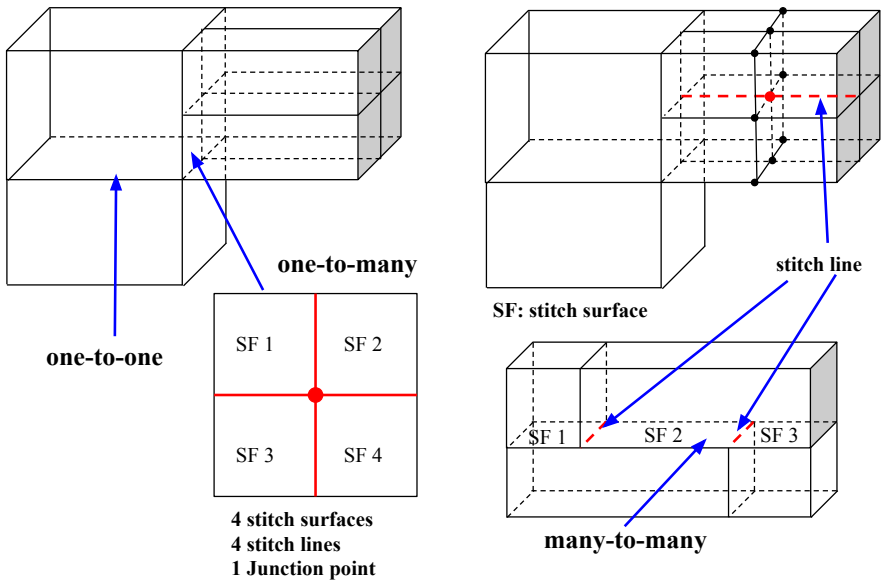

Fig. 4 Construction of stitch surfaces.

match exactly and have the same size. 2) One-to-many matching. This is the situation when one block boundary is attached to more than one blocks but its size is equal to the summation of the sizes of these block boundaries. 3) Many-to-many matching. This is the situation when two groups of block boundaries have the same size.

A block boundary is represented by two families of intersecting lines and these lines form the surface mesh for this block boundary. The size of a block boundary is defined as the pair (n_i, n_j). n_i and n_j are the number of lines in each family. Figure 4 demonstrates three ways in which stitch surfaces can be built. The figure on the top-left illustrates the one-to-one and one-to-many matchings. Many-to-many matching is shown in the bottom-right of the figure. One-to-many and many-to-many matchings avoid the generation of small blocks. This reduces the total number of blocks, stitch surfaces, stitch lines and junction points, and provides more freedom in designing block layouts. The final stitch surfaces of the 3D blocks for a stator blade is illustrated in Fig. 5.

C. 3D Elliptic Smoothing

After all the blocks are generated and all the stitch surfaces, stitch lines and junction points are identified, 3D elliptic smoothing is used to remove grid folding and improve the mesh quality. The

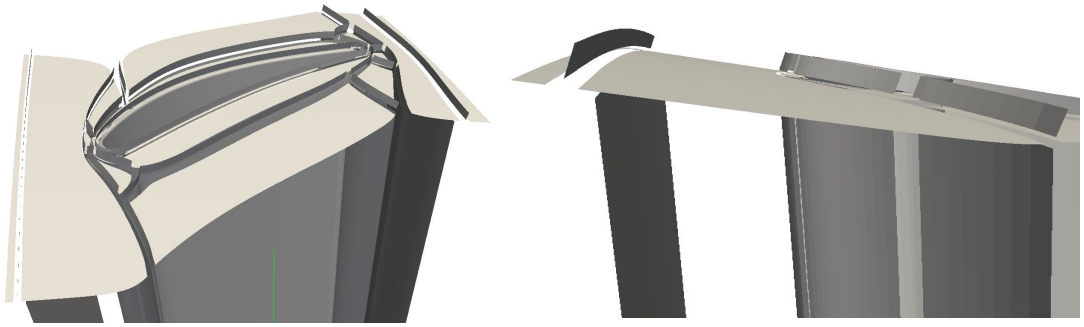

a) b)

Fig. 5 Stitch surfaces for a stator blade.

smoothing process solves the elliptic system in Eq. (1).

$$\sum_{m=1}^{m=3}\sum_{n=1}^{n=3} g^{mn}\mathbf{x}_{\xi^m\xi^n} + \sum_{n=1}^{n=3} P_n g^{nn}\mathbf{x}_{\xi^n} = 0 \tag{1}$$

Eq. (1) is discretized by central differencing and the resulting linear system is solved by the Jacobi method. Source functions P_n are computed on the blade surface and endwalls to enforce grid orthogonality and spacing for viscous flow simulations. For the details of the procedure, readers can refer to the work by Thompson [10].

For a stitch line, elliptic smoothing can not be applied because the number of blocks sharing this line is not necessarily equal to 4. Weighted Laplacian smoothing is used instead. The stencil for the weighted Laplacian smoothing is built in such a way that only the points on the surface normal to the direction of the stitch line is included. This is shown in Fig. 4. The stitch line is highlighted as the dashed red line and the black dots represent the stencil used for the weighted Laplacian smoothing. Junction point are smoothed by the weighted Laplacian smoothing as well but all their neighbouring points are used for the smoothing.

The periodic surfaces are also smoothed and our experiences show that this procedure is essential. Since modern turbomachinery blades are designed in a 3D approach [11, 12], the meshes on the periodic surfaces have to be smoothed to follow the shape of the blade along the span in order to improve the mesh quality. The mesh points on the periodic surface are all treated as junction points. Figure 6 shows the meshes on the periodic surfaces which bow and twist in the same fashion as the blade along the span. The smoothing of the periodic boundaries is found to be crucial to

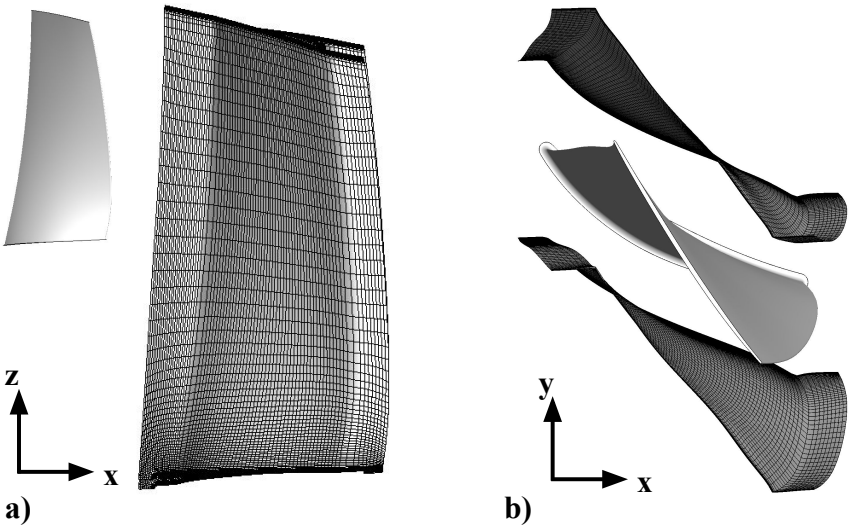

Fig. 6 Meshes on periodic surfaces.

improve the robustness of the method and yield a high quality mesh.

It is noted that the current method automatically smooths not only the interior nodes of all blocks, but also the surfaces, lines and nodes that are shared by the blocks. The advantage of this strategy is that users only need to choose the adequate block layout and parameters to decide the mesh spacing on the boundaries, coordinates of interior nodes and nodes on the periodic boundaries are solutions of Eq. 1. This will maximize the mesh quality meanwhile minimize the human interventions on meshing turbomachinery blade passages. Figure 7 shows the mesh on the mid-span and around the blade fillets. The figure demonstrates that the final positions of the interior nodes (including the ones on the periodic boundaries) are independent of their initial positions. Figure 8 shows a stator blade whose shape along the span has been distorted in the purpose of demonstrating the robustness of the smoothing method. The initial mesh has sever grid foldings. After the elliptic smoothing the grid foldings are eliminated, the positions of the blocks are adjusted to achieve optimum mesh quality, and the periodic boundaries are updated to take into account the distortion of the blade along the span.

D. Post-Refinement of Boundary Layer Meshes

The procedure in Sec. II C might encounter difficulties in practice when a fine boundary layer mesh is generated around a concave region (e.g. the blade fillet). Figure 9 a) shows the mesh

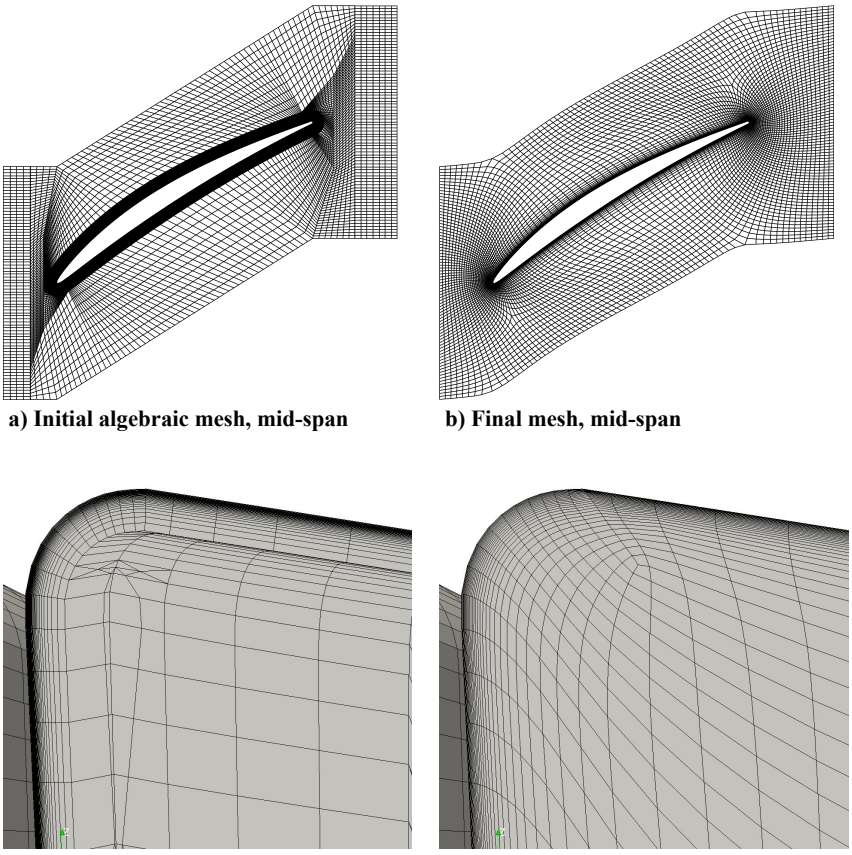

Fig. 7 Meshes on periodic surfaces.

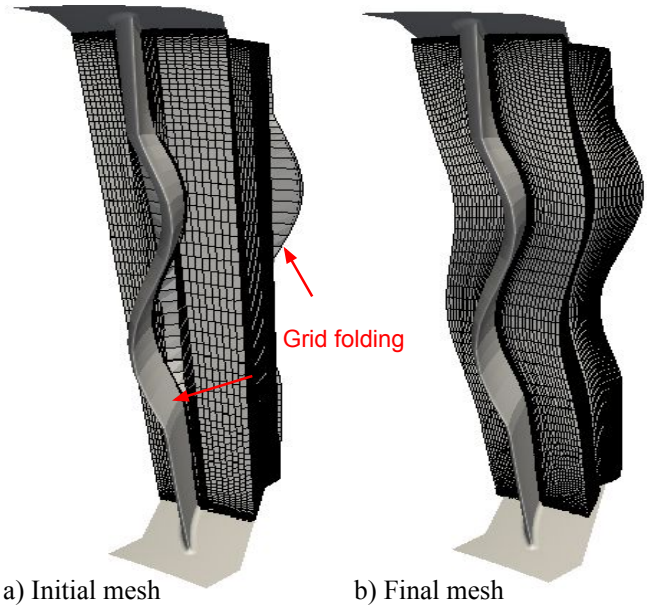

Fig. 8 Stator blade with distorted shape along the span.

around the hub fillet when there are fewer number of layers in the boundary layer mesh. With the number of layers in the boundary layer mesh block doubled, the mesh around the hub fillet is shown in Fig. 9 b). It can be observed that the domain occupied by the boundary layer mesh is inflated and low quality hexahedra are generated in the region highlighted in the blue dashed line. This is mainly caused by the fact that the source functions on the boundaries are interpolated linearly to the interior of the blocks by TFI [10]. One could improve this by using a non-linear interpolation. However, based on extensive tests such approach is found to be less robust.

The other option is to generate a boundary layer mesh with a fraction of the specified number of layers in the first place. This coarse boundary layer mesh is saved as a background mesh and a finer boundary layer mesh is then generated by interpolation. This is illustrated in Fig. 9 d). The dashed lines and hollow dots represent the initial coarse boundary layer mesh. The solid lines and dots represent the final finer boundary layer mesh. Since boundary orthogonality is already satisfied by the background mesh, the fine boundary layer mesh is also orthogonal near the wall and mesh expansion ratio can be controlled directly through the interpolation. Figure 9 c) shows the mesh using this refinement method and compared to Fig. 9 b) the mesh quality has been improved significantly.

III. Results

The method has been implemented in the in-house meshing tool [4], which is routinely applied to the design and analysis of turbomachinery blades. Two test cases are presented to demonstrate the benefit of the proposed method in improving mesh quality for blade passages with blade and platform fillets. The first test case is the NASA Rotor 37 and the second test case is an industrial multi-stage shrouded compressor in a high speed machine.

For convenience in the following texts, the mesh generated by the current method is referred as "3D mesh" and the mesh generated by any 2.5D approach is referred as "2.5D mesh".

A. CFD Solver

The CFD simulations in this paper are performed with the in-house CFD code. The details of the code can be found in [13, 14] and a brief description is provide here. The code uses a cell-centred

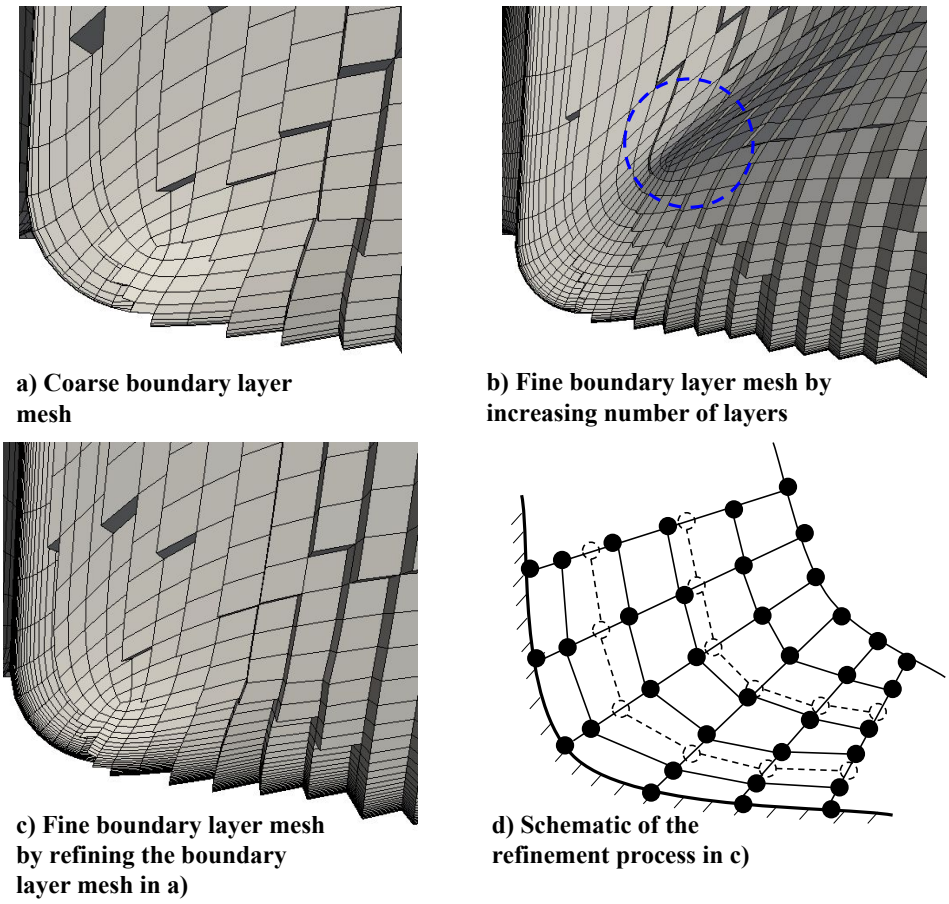

Fig. 9 Generation of boundary layer meshes.

finite volume approach to solve the unsteady Reynolds Averaged Navier-Stokes (RANS) equations on unstructured meshes. Steady solutions are obtained by pseudo time marching. The unsteady RANS equations in the differential form read:

$$\begin{aligned} \frac{\partial \overline{\rho}}{\partial t} + \frac{\partial (\overline{\rho}\tilde{v_i})}{\partial x_j} &= 0 \\ \frac{\partial (\overline{\rho}\tilde{v_i})}{\partial t} + \frac{\partial (\overline{\rho}\tilde{v_i}\tilde{v_j})}{\partial x_j} &= -\frac{\partial \overline{p}}{\partial x_i} + \frac{\partial}{\partial x_j}(\tilde{\tau_{ij}} + \tau_{ij}^t) \\ \frac{\partial (\overline{\rho}\tilde{E})}{\partial t} + \frac{\partial (\overline{\rho}\tilde{v_j}\tilde{H})}{\partial x_j} &= \frac{\partial}{\partial x_j}(\kappa \frac{\partial \tilde{T}}{\partial x_j} + \tilde{v_i}(\tilde{\tau_{ij}} + \tau_{ij}^t)) \end{aligned} \tag{2}$$

Where,

$$\tilde{\tau_{ij}} = 2\mu(\tilde{S_{ij}} - \frac{1}{3}\frac{\partial \tilde{v_k}}{\partial x_k}\delta_{ij}), \quad \overline{p} = (\gamma - 1)\overline{\rho}(\tilde{E} - \frac{1}{2}\tilde{u_j}\tilde{u_j}), \quad \kappa\frac{\partial T}{\partial x_j} = \frac{\gamma}{\gamma - 1}\frac{\mu}{P_r}\frac{\partial}{\partial x_j}(\frac{\overline{p}}{\overline{\rho}}), \tag{3}$$

The tilde "$\sim$" and overbar "$-$" represent Favre averaging and Reynolds averaging respectively.

The working fluid is air and it is treated as calorically perfect gas. γ and the Prandtl number P_r is held constant at 1.4 and 0.72. μ is evaluated using the Sutherland's law (using a reference viscosity of $1.7894 \times 10^{-5} \frac{kg}{ms}$) , reference temperature 288.15K and Sutherland's constant 110K). If the Boussinesq assumption holds, the Reynolds stress τ_{ij}^t can be written as a linear function of the mean flow gradient: $2\mu_t(\tilde{S_{ij}} - \frac{1}{3}\frac{\partial \tilde{v_k}}{\partial x_k}\delta_{ij})$. Otherwise there is a non-linear constitutive relation between the Reynolds stress and the mean flow gradient [15].

The code is formally 2^{nd} order accurate in space and time. The numerical flux is evaluated using the Monotonic Upstream-centered Scheme for Conservation Laws (MUSCL) scheme with the van Albada limiter [16]. The gradients are evaluated using weighted least squares [17]. Inviscid flux is computed by Roe's Riemann solver [16]. By default the Wilcox $k-\omega$ turbulence model is used [18] in the solver. The solver automatically switches between the wall function approach and low-Re approach depending upon the y^+ of the cells immediately close to the wall.

B. Test Case - Rotor 37

NASA Rotor 37 is an axial compressor rotor blade with 36 blades passages. The tip clearance is 2.5% of the span and is assumed to be constant from the leading edge to the trailing edge. Readers can refer to Dunham [19] for more details.

The 3D mesh using the current package and 2.5D meshes using the commercial package and the current meshing package are compared. The hub fillet is added deliberately to study the effect of fillet truncation on the blade performance. The fillet radius is set to be 3mm and it remains constant from the leading edge to the trailing edge on the hub. The truncation angle of the fillet for the 2.5D meshes is set to 20^0 for the current package and the commercial package. Figure 10 a) and b) show the 2.5D meshes from the current package and the commercial package respectively. Because the cut plane is not necessarily aligned with the mesh contours, some hexahedra are missing in the figure. Nonetheless, it can be clearly seen that: 1) The mesh lines from both packages are no longer orthogonal to the viscous wall around the fillet. 2) Both packages generate skewed elements around the fillet; 3) The 2.5D meshes from the current package and the commercial package are extremely similar. Figure 10 c) shows the 3D mesh using the proposed method. The drawbacks of the 2.5D meshing technique observed above are eliminated. The meshes are always orthogonal to the viscous

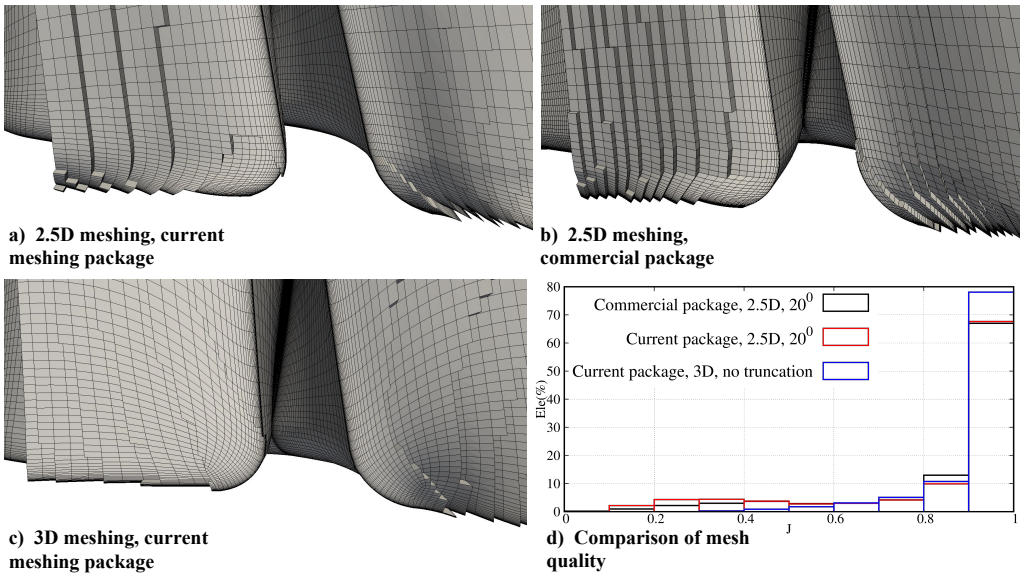

Fig. 10 2.5D and 3D meshes around the hub fillet for Rotor 37.

walls and no skewed elements are generated around the region where the blade and the hub meet. For the meshes around the tip gap regions, the meshes from the 3D mesh and the 2.5D meshes from the current and commercial package are extremely similar. This is demonstrated in Fig. 11.

Figure 10 d) shows the mesh quality in terms of scaled Jacobian J. J is a measure of the proximity of a hexahedron to a cube. If J is equal to 0, a hexahedron degenerates into a planar element. If J is equal to 1, a hexahedron becomes a cube. The histogram of the scaled Jacobian shows that the 2.5D meshes from both the current package and the commercial package have comparable quality. The 3D mesh has a considerably higher mesh quality. This is because the skewed elements around the fillet and the hub has been removed. Besides, it can seen that the 2.5D mesh from the current package has comparable quality to the 2.5D mesh from the commercial package. Therefore the 2.5D meshes from the current package can be considered to be representative of the 2.5D meshes generated from other resources. In the following study, only the 2.5D meshes from the current package are used.

Three sets of simulations are prepared to show the effect of the truncated fillet. They use a 3D mesh with no truncated fillet, a 2.5D mesh with a fillet truncation angle of 20^0 and a 2.5D mesh with a fillet truncation angle of 45^0. Mesh sensitivity study is conducted at the operating point near the peak efficiency. Three levels are meshes are used. The coarse mesh has around 0.8 million

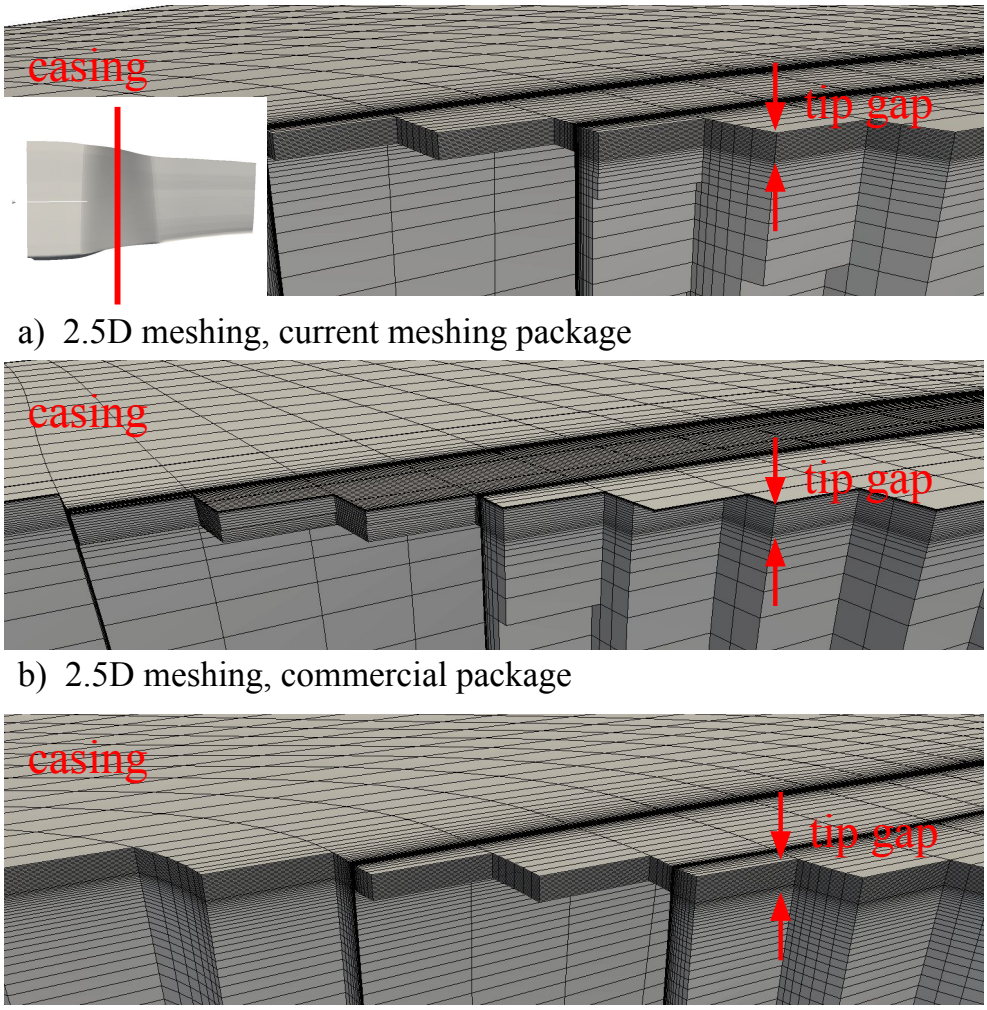

Fig. 11 2.5D and 3D meshes around the tip gap for Rotor 37.

elements, the medium level has around 1.3 million elements and the fine mesh has around 1.9 million elements. The predicted efficiency is summarised in Table 1. The table shows that the efficiency changes marginally by increasing the mesh sizes. The mesh with the medium size is then used.

At this operating point, the effect of the truncated fillet on the flow fields of Rotor 37 is first shown in Fig. 12. Relative total pressure coefficient is evaluated in the frame of reference associated with the blade and computed as the difference between the local total pressure and the inlet total pressure and then normalised by the inlet total pressure. The contour plots are extracted on a plane 10% chord downstream the trailing edge.

From Fig.12 it can be clearly seen that the 2.5D meshes with truncation angles of 20^0 and 45^0

Table 1 Mesh sensitivity study of adiabatic efficiency for Rotor 37.

	Coarse	Medium	Fine
2.5D, 20^0	86.01	86.04	86.06
2.5D, 45^0	86.12	86.14	86.15
3D	86.27	86.29	86.3

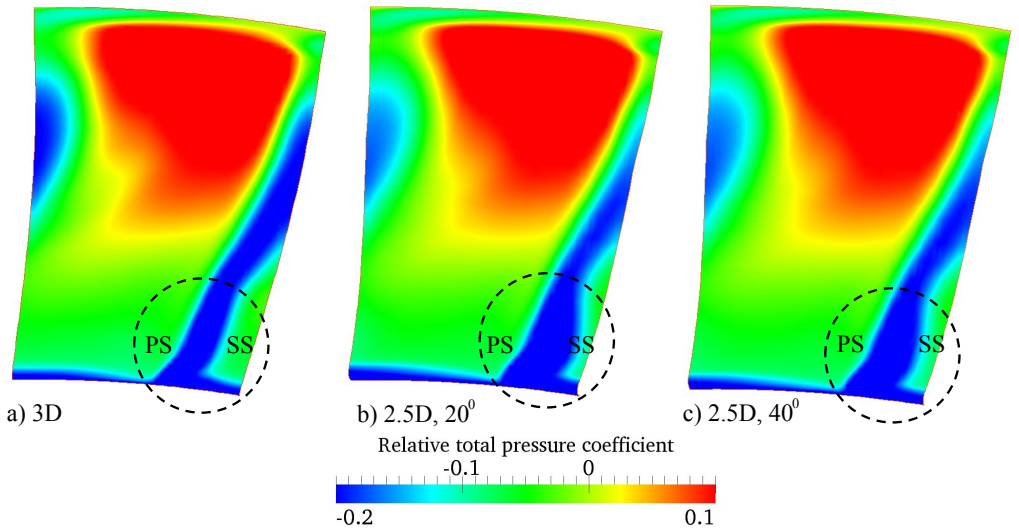

Fig. 12 2.5D and 3D meshes around the hub fillet for Rotor 37.

lead to a stronger wake on the suction side towards the hub. This is because truncating the fillet modifies the endwall geometry and this lead to a slightly different prediction of the corner stall on the suction side. The simulation using the 3D mesh yields a weaker corner stall on the suction side towards the hub.

As is shown in the Fig. 12, the simulations using the 2.5D mesh yield a stronger hub corner stall, which results in more losses. Its impact on the overall performance can be seen in Tabel 1. The simulation using the 3D mesh yields a slightly higher efficiency. A complete view of this effect on the performance can be seen in Fig. 13. The simulation using the 3D mesh predicts higher total-to-total pressure ratio and efficiency for a given massflow compared to the simulations using 2.5D meshes. The under-estimated efficiency by all the CFD solutions is due to the fact that the experimental probes are not close enough to the endwalls and the endwall losses are under-estimated in the experimental data [20]. The over-predicted pressure ratio could be beucase the shroud leakage slot in front of the leading edge is not inclued in the model. Better agreement with the experimental

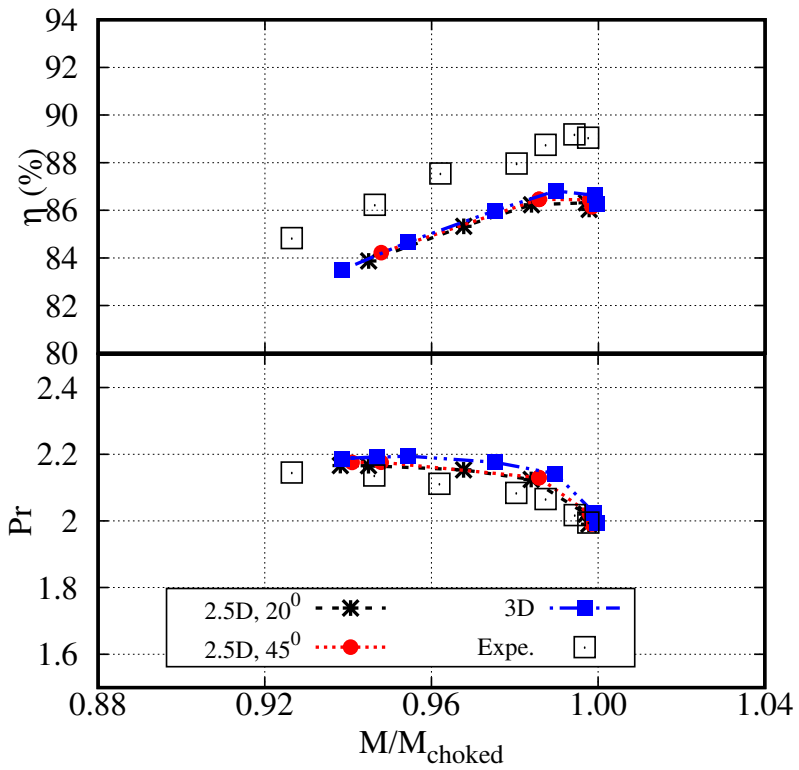

Fig. 13 Compressor map for Rotor 37.

data is observed by including this leakage flow. Interested Readers can refer to Shabbir et al [21] for more details. Nonetheless, the comparison demonstrated that truncated fillets have negative effects on the performance.

C. Test Case - Multistage Compressor

The second test case is a multi-stage shrouded compressor in a high speed machine. The compressor (see Fig. 14) has 19 blade-rows and 7 shroud cavities below the stators of the first 7 stages. The first three stages have provisions of stator variable vanes to improve compressor performance at part speeds. The challenge of this industrial geometry is that the platform have fillets on the platform and at middle and rear stages the blade fillet on the leading edge is on or close to the platform, which is shown in Fig. 16 a). This cause difficulties for the 2.5D meshing technique.

This difficulty can be illustrated by Fig. 15, which shows the projection of the 2.5D meshes on the meridional plane around the leading edge of a blade. For the 2.5D meshing technique, truncation of the platform fillet or coarsening the mesh around the platform fillet is needed in order to avoid

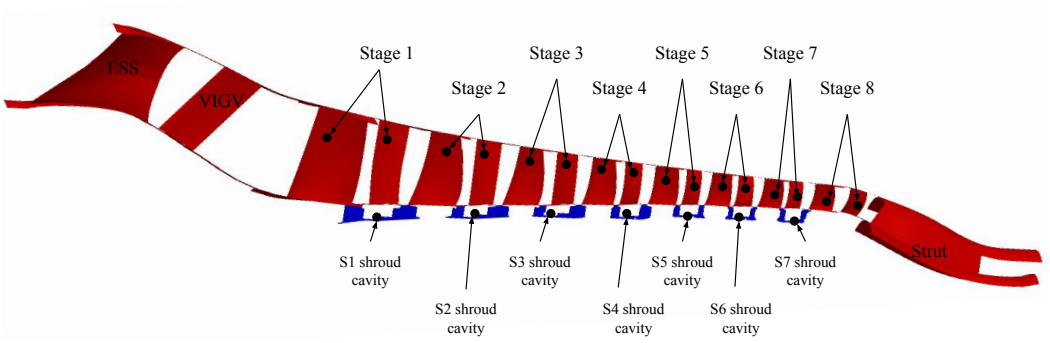

Fig. 14 Schematic of the compressor.

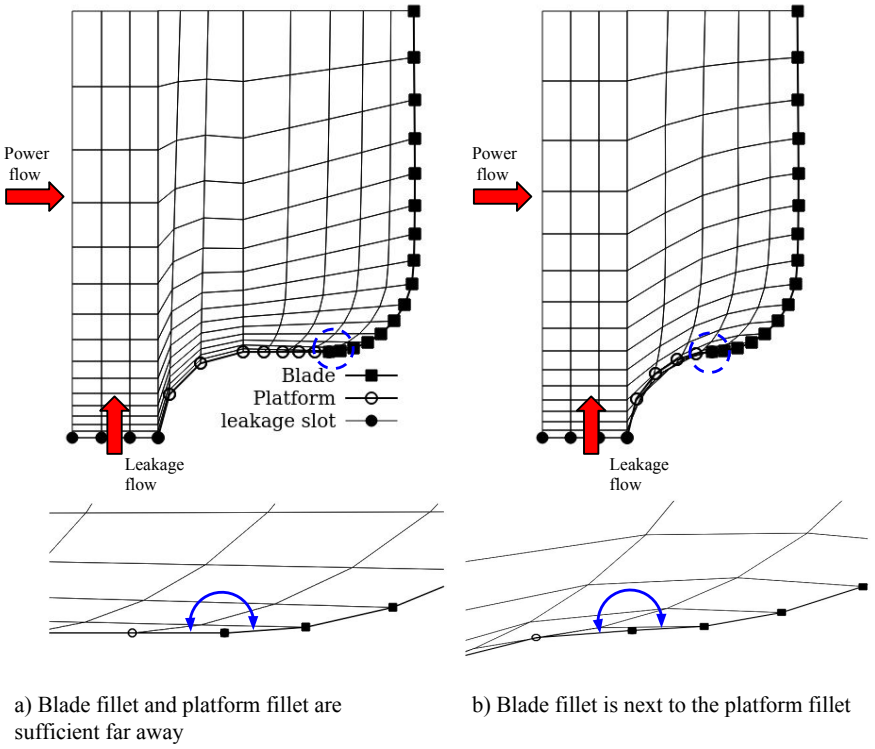

Fig. 15 Schematic of mesh projection on the meridional plane.

generating highly skewed elements or 3D smoothing should be used to improve the mesh quality around this region. The mesh elements around the junction where the blade and the hub meets can still remain acceptable if the blade fillet is truncated and it is sufficiently far away from the platform fillet, which is illustrated in Fig 15 a). However, when the blade fillet is close or on the platform fillet, elements with $J \leq 0$ could be generated. This is illustrated by in Fig. 15 b). The quality of these elements can hardly benefit from 3D smoothing because their quality is bounded by the geometry. This is highlighted by the blue arrows in Fig. 15. One has to carefully modify the

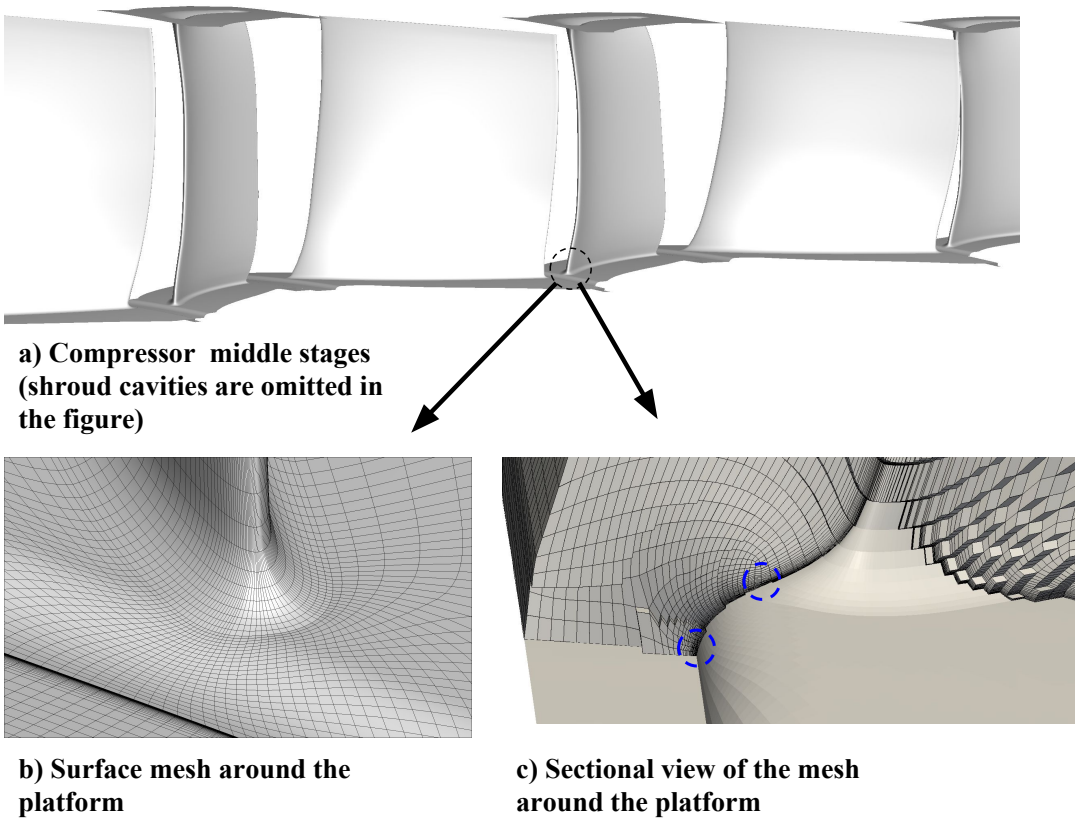

Fig. 16 Mesh around the blade platform.

geometry (e.g. extend the platform, modify the shape of the platform, or increase the truncation angle of the fillet) to generate a valid mesh using the 2.5D meshing technique.

However, the limitation of the 2.5D technique can be overcome by the proposed method. Figure 17 shows the mesh detail around a variable stator vane where there are sufficient space between the blade and the leakage slot. Figure 16 b)-c) show the more challenging scenario where the blade leading edge is on the platform fillet. The figures present the surface mesh and a sectional view of the volume mesh around the platform leading edge respectively. An optimal mesh is generated for this challenging geometry.

Before presenting the simulations of the whole compressor, it is beneficial to show the impact of truncated blade fillets and platform fillets on the flow field with the presence of shroud leakage flow. A stator variable vanes is chosen for this study, because the blade is sufficiently far away from the platform so that a 2.5D mesh with reasonable quality can be generated. A schematic of this study is shown in Fig. 18. Only the stator blade is modelled and its computational domains are highlighted

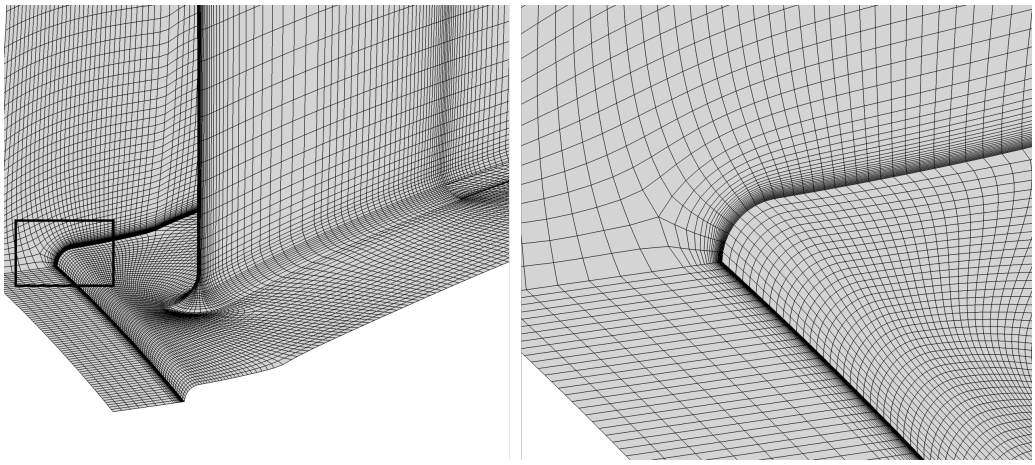

Fig. 17 Mesh details around S1 inlet.

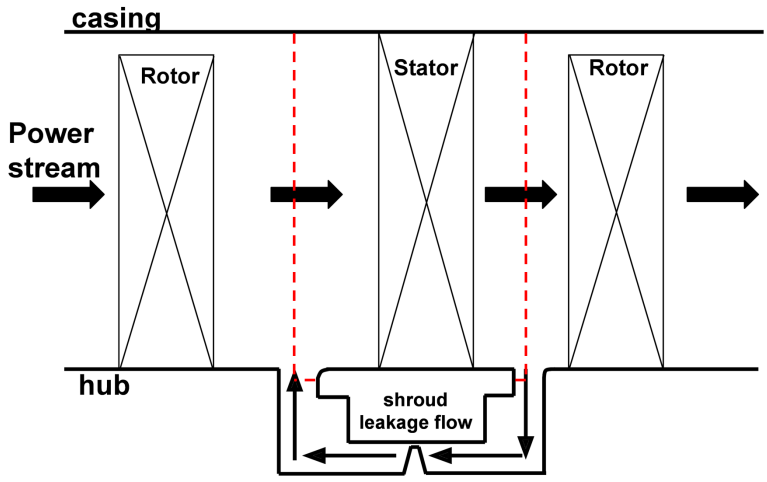

Fig. 18 Schematic of a stator with a shroud cavity.

in the red dashed line in Fig. 18. Identical boundary conditions are applied to both 2.5D and 3D meshes and their values are extracted from a multi-stage compressor simulation at the design point. All the flow properties are extracted at the position which is 5% of the chord length upstream of the leading edge. The radial profiles are generated by mass-averaging in the circumferential direction along the span.

The platform fillet is truncated with an angle of 45^0 in the first place to show the effect of the truncated fillet on the radial flow angles upstream of the leading edge. This geometry is used for both the 3D and 2.5D meshes. Three set of meshes are used to ensure that the solution is not sensitive to mesh sizes. Apart from refining the mesh close to the wall, the mesh on the platform

Table 2 Mesh statistics of the stator blade with shroud leakage slots.

	Coarse		Medium		Fine	
	No. Ele	y^+	No. Ele.	y^+	No. Ele	y^+
2.5D mesh	616368	≈50	1168000	≈5	2262040	≈0.5
3D mesh	662056	≈50	1203304	≈5	2143632	≈0.5

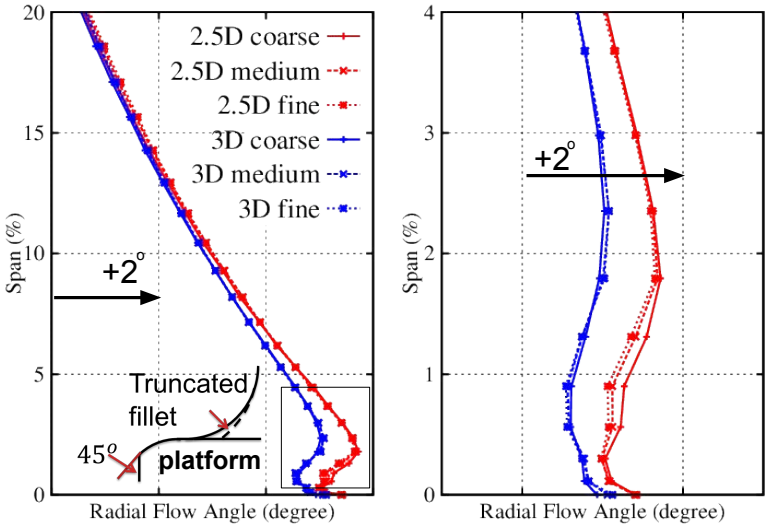

Fig. 19 Drawback of truncated platform using the 2.5D approach.

fillet is also refined. 5, 10, and 20 points are put on the fillet of the platform. The statistics of the meshes are summarized in Table 2. Figure 19 shows the mass-averaged radial flow angles 5% chord upstream of the blade leading edge along the span. It is interesting to notice that although both meshes share the same geometries of the platform, the 3D mesh yields smaller radial flow angles than the 2.5D mesh towards the hub. The largest difference is roughly 0.8^o around 2% span. This is due to the fact that the 2.5D mesh also has a truncated fillet. This modifies the shape of the blade close to the hub and changes the potential flow field in front of the leading edge.

A further comparison (see Fig. 20) is made between the simulations using the 3D mesh which has no truncations on the blade and the platform fillets and the one using the 2.5D mesh which has a truncation angle of 45^0 both on the platform and blade fillets. The comparison shows that close to the hub there is a difference of more than 1^0 on the radial flow angle. This is an combined effect of the truncated blade fillet and the platform fillet: the truncated fillet modifies the potential flow field in front of the leading edge close to the hub and the leakage flow enters the power stream more

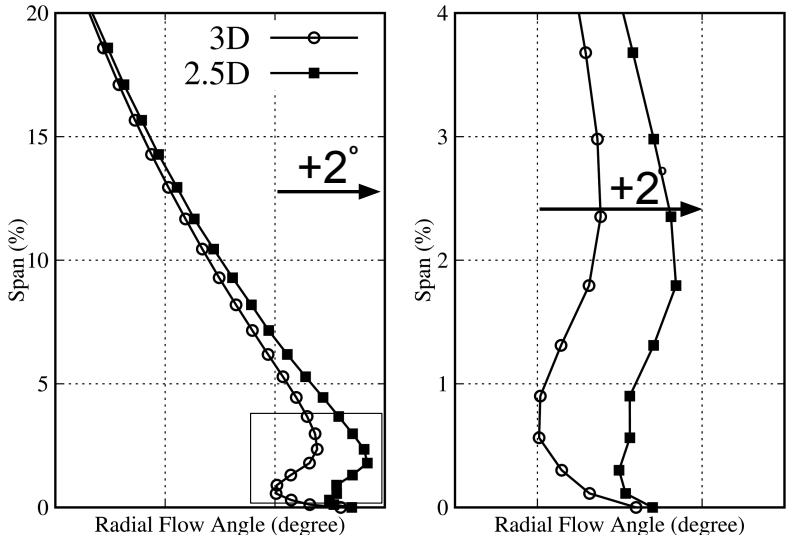

Fig. 20 Variation of radial flow angles using 3D and 2.5D meshes.

abruptly when the truncated angle is applied to the platform fillet, .

The effect of the truncated fillet on the compressor are demonstrated by two simulations. The geometries in both simulations contain all the blade rows but don't have penny gaps and shroud cavities. Only blade fillets are included. Therefore the differences in the flow fields and performance is due to the truncation of the fillet. The choice of mesh sizes is guided by the mesh dependence studies in previous sections. The mesh size for each passage is around 1 million and the targeted y^+ on the wall is ≈ 1. Figure 21 shows the total pressure coefficient at the exit boundary of a stator in front and rear stages at the design point. Unlike the Rotor 37 case, there is no corner separations around the endwall regions. However, one could still observe that the truncated fillet generates a stronger wake close to the endwall regions especially close to the casing at both stator exit boundaries. Although the difference is small, the accumulation across the stages leads to a reduction of around 0.15% of the mass flow and 0.11% in adiabatic efficiency for the simulations using 2.5D meshes.

Finally the whole compressor are simulated with shroud cavities included. As is demonstrated in Fig. 20, the 2.5D approach face difficulties in meshing the blade passages in the middle and rear stages. The platforms of the middle and rear stages are extended where neccessary to allow meshes with reasoanble quality to be generated. An Explicit Algebric Reynolds Stress Model (EARSM) is used in this simulation due to its superior behaviour for flows under adverse pressure gradient [15].

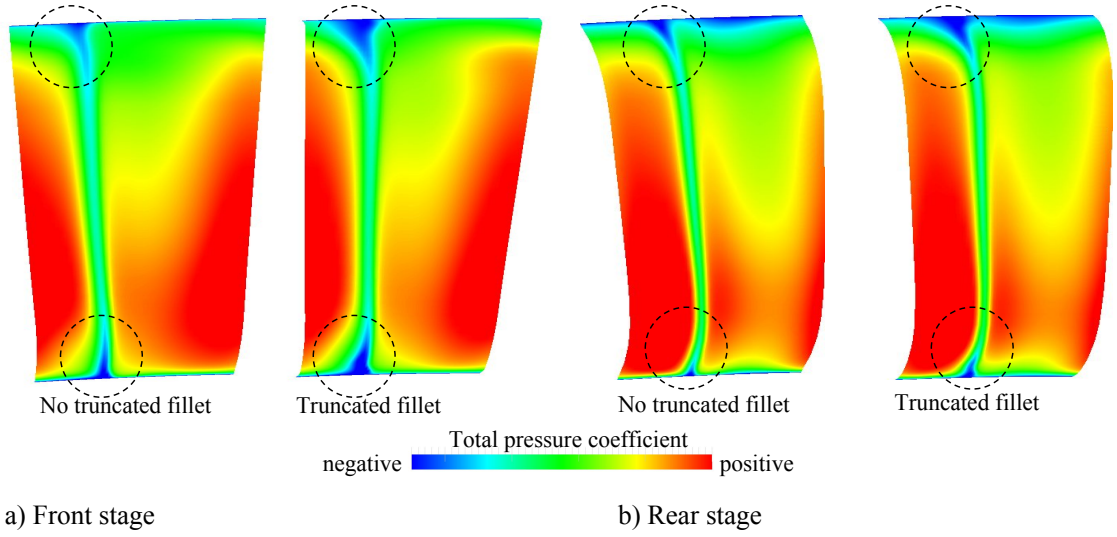

Fig. 21 Schematic of a stator with a shroud cavity and flow directions at the inlet.

The details of the model can be found in [15] and no turning is applied to the model. Only one passage of each blade row is modelled and blade rows are coupled using the mixing plane approach. The choice of mesh sizes is guided by the mesh dependence studies in the stator blade. The mesh size for each passage is around 1 million and the targeted y^+ on the wall is ≈ 1. A more detailed grid sensitivity study can be found in Wang et al [22].

The predicted compressor map is shown in Fig. 22. It can be seen that with the same mass flow the simulation using the 2.5D meshes predicts a lower total-to-total pressure rise. The losses in total pressure is the combined effects of the truncated blade and platform fillets. Besides, the extension of the platform reduces the area of the leakage slot and the mass flow of the leakage air is largely determined by the knife clearance of the labyrinth seal, therefore the leakage air enters the power stream at a higher velocity due to the reduced slot area. This amplifies the effect of the leakage air and generates more losses. Figure 23 shows the entropy contour lines at the exit of rotor 3 at the high working line. It can be seen that the entropy contour with the 2.5D mesh are shift radially compared to the one with the 3D mesh. This is because the solutions with the 2.5D mesh predict the shroud leakage air with a larger radial flow angle, which is demonstrated in previous sections. At the stator 4 inlet, the radial profiles of total pressure is presented in Fig. 24. The data are extracted at the position 5% chord upstream of the stator leading edge. It can be seen that the simulation using the 2.5D mesh over-estimated the losses by the shroud cavities towards the hub

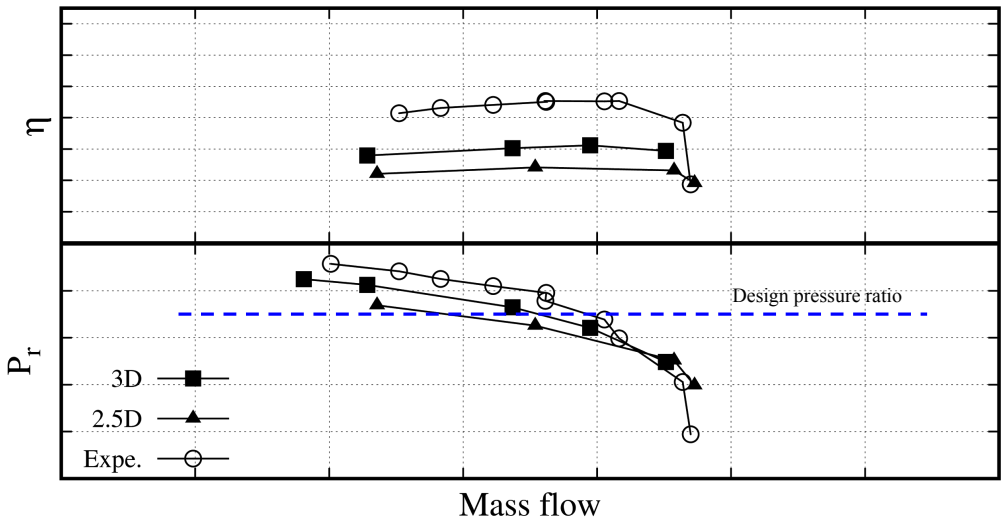

Fig. 22 Compressor map.

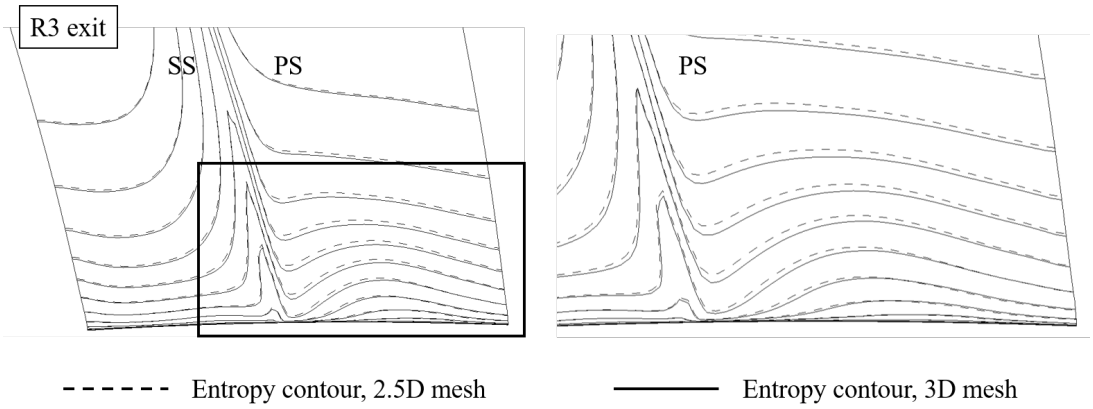

Fig. 23 Entropy contour at R3 exit at high working line.

while the one using the 3D mesh has a more reasonable prediction.

IV. Conclusions and Future Work

This paper has described a method to generate 3D multi-block structured meshes in the turbomachinery blade passages. The aim is to mesh endwall geometrical features accurately with optimal mesh quality. This will improve the accuracy and the reliability of CFD in predicting the performance and flow fields of blade passages.

3D blocks are directly generated in the blade passage. The surfaces, lines and points which join the blocks together are automatically identified. Elliptic smoothing is used to remove grid folding and improve mesh quality for each block and block interfaces. The robustness of the method is

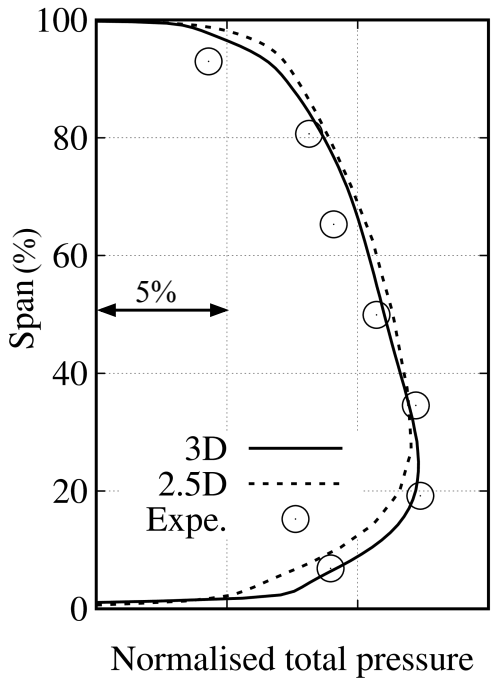

Fig. 24 Radial profiles of total pressure at the S4 inlet.

enhanced by smoothing the periodic boundaries and a novel technique to refine the boundary layer meshes.

The case of Rotor 37 shows that the mesh quality is greatly improved by the proposed method. This is because the skewed elements around the hub region due to truncated fillets have been eliminated. The truncated fillet is found to yield a stronger hub corner stall in the CFD solutions compared to the one using the 3D mesh. In terms of overall performance, the simulations using the truncated has a negative impact on the overall performance and they predict a slightly lower pressure ratio and efficiency compared to the ones using the 3D mesh.

For the multistage compressor, the simulation using truncated platform and blade fillets yields larger radial flow angle in front of the leading edge. Truncation of the fillet leads to a slightly stronger wake on the endwall region, especially towards the casing. This difference is accumulated across the stages and leads to a drop of 0.15% in mass flow and 0.11% in efficiency at the design point. For the simulations with all the shroud cavities included, the one using the 2.5D mesh predicts a lower pressure ratio and efficiency compared to the one using the 3D mesh. This is supported by plotting the radial profiles of total pressure upstream of a stator in a middle stage, it shows that

the simulation using the 2.5D shows predicts larger losses towards the hub.

Acknowledgment

The authors are grateful to Rolls-Royce plc for funding this work under the SIMulation Off-Design (SIMOD) project and granting permission for its publication.

References

[1] Thompson, J. E., Warsi, Z., and Mastin, C. W., *Numerical Grid Generation Foundations and Applications*, Elsevier Science Publishing Co., Inc., New York, NY, USA, 1985.

[2] Sbardella, L., Sayma, A. I., and Imregun, M., "Semi-Structured Meshes for Axial Turbomacinery Blades," *International Journal of Numerical Methods in Fluids*, Vol. 32, No. 5, 2000, pp. 569–584. doi:10.1002/(SICI)1097-0363(20000315)32:5<569::AID-FLD975>3.0.CO;2-V.

[3] Shahpar, S. and Lapworth, L., "PADRAM: Parametric Design and Rapid Meshing System for Turbomachinery Optimization," *Proceedings of ASME Turbo Expo 2003*, No. GT2012-69030, 2003, pp. 2135–2148. doi:10.1115/GT2003-38698.

[4] Wang, F., *Whole Aero-Engine Meshing and CFD Simulation*, Ph.D. thesis, Imperial College London, London, UK, 2013.

[5] Rosic, B., Denton, J. D., and Pullan, G., "The Importance of Shroud Leakage Modeling in Multistage Turbine Flow Calculations," *Journal of Turbomachinery*, Vol. 130, No. 4, 2008, pp. 1–10. doi: 10.1115/1.2181999.

[6] Wellborn, S. and Okiishi, T., "The Influence of Shrouded Stator Cavity Flows on Multistage Compressor Performance," *Journa of Turbomachinery*, Vol. 121, No. 3, 1999, pp. 486–497. doi:10.1115/1.2841341.

[7] Wang, F. and di Mare, L., "Hybrid Meshing Using Constrained Delaunay Triangulation for Viscous Flow Simulations," *International Journal for Numerical Methods in Engineering*, Vol. 3, No. 1, 2016, pp. 1–22. doi:10.1002/nme.5272.

[8] Zagitov, R. A., N.Dushko, A., and Shmotin, Y. N., "Automatic Three Dimensional Grid Generation In Turbo Machine Blade Passages," *Proceedings of ASME Turbo Expo 2014*, No. GT2014-27127, 2014, pp. 2111–2118. doi:10.1115/GT2014-27127.

[9] Smith, R. E., "Transfinite Interpolation Generation Systems," *Handbook of Grid Generation*, chap. 3, CRC Press, Florida, USA, 1998.

[10] Thompson, J., Thames, F., and Mastin, C., "Automatic Numerical Generation of Body-fitted Curvilinear Coordinates System for Field Containing Any Number of Arbitrary Two-Dimensional Bodies,"

Journal of Computational Physics, Vol. 15, No. 3, 1974, pp. 299–319. doi:10.1016/0021-9991(74)90114-4.

[11] Gallimore, S. J., Bolger, J. J., Cumpsty, N., Taylor, M. J., Wright, P. I., and Place, J. M. M., "The Use of Sweep and Dihedral in Multistage Axial Flow Compressor Blading-Part I: University Research and Methods Development," *Journal of Turbomachinery*, Vol. 124, No. 4, 2002, pp. 521–532. doi: 10.1115/1.1507333.

[12] Gallimore, S. J., Bolger, J. J., Cumpsty, N., Taylor, M. J., Wright, P. I., and Place, J. M. M., "The Use of Sweep and Dihedral in Multistage Axial Flow Compressor Blading-Part II: Low and High-Speed Designs and Test Verification," *Journal of Turbomachinery*, Vol. 124, No. 4, 2002, pp. 533–541. doi:10.1115/1.1507334.

[13] di Mare, L., Y.Kulkarni, D., Wang, F., Romanov, A., Ramar, P. R., and Zachariadis, Z. I., "Virtual Gas Turbine: Geometry and Conceptual Description," *Proceedings of ASME TurboExpo 2011*, No. GT2011-46437, 2011, pp. 347–358. doi:10.1115/GT2011-46437.

[14] Carnevale, M., Wang, F., Green, J., and di Mare, L., "Lip Stall Suppression in Powered Intakes," *Journal of Propulsion and Power*, Vol. 32, No. 1, 2015, pp. 161–170. doi:dx.doi.org/10.2514/1.B35811.

[15] Menter, F., Garbaruk, A., and Egorov, Y., "Explicit Algebraic Reynolds Stress Models for Anisotropic Wall-Bounded Flows," *Progress in Flight Physics*, Vol. 3, 2012, pp. 89–104. doi: http://dx.doi.org/10.1051/eucass/201203089.

[16] Hirsch, C., *Numerical Computation of Internal and External Flows, Volume 2, Computational Methods for Inviscid and Viscous Flows*, Wiley, Baffins Lane, West Sussex, England, 1990.

[17] Mavriplis, D. J., "Revisiting the Least Squares Procedure for Gradient Reconstruction on Unstructured Meshes," Tech. Rep. NASA/CR-2003-212683, NASA, Hampton, Virginia, USA, 2003.

[18] Wilcox, D. C., "Reassessment of the Scale-Determining Equation for Advanced Turbulence Models," *AIAA Journal*, Vol. 26, No. 11, 1988, pp. 1299–1310. doi:dx.doi.org/10.2514/3.10041.

[19] Dunham, J., "CFD Validation for Propulsion System Components," Tech. Rep. AGARD-AR-355, AGARD, Hull, Canada, May 1998.

[20] Denton, J., "Lesson from Rotor 37," *Journal of Thermal Science*, Vol. 6, No. 1, 1996, pp. 1–13. doi: doi:10.1007/s11630-997-0010-9.

[21] Shabbir, A., Celestina, M., Adamczyk, J., and Strazisar, A., "The Effect of Hub Leakage Flow on Two High Speed Axial Flow Compressor Rotors," *Proceedings of the 1997 ASME Turbo Expo*, No. 97-GT-346, Orlando, Florida, USA, June 1997, pp. 1–14. doi:doi:10.1115/97-GT-346.

[22] Wang, F., Carnevale, M., di Mare, L., and Gallimore, S., "Simulation of Multi-stage Compressor at Off-Design Conditions," *Proceedings of ASME Turbo Expo 2017*, No. GT2017-64964, Charlotte, USA, June 2017, pp. 1–11.